Materials Chemistry and Physics 248 (2020) 122903

Contents lists available at ScienceDirect

Materials Chemistry and Physics

journal homepage: www.elsevier.com/locate/matchemphys

Synthesis of high value-added Na–P1 and Na-FAU zeolites using waste glass from fluorescent tubes and aluminum scraps

Mouna Sayehi [a,*], Gabriella Garbarino [b], Gérard Delahay [c], Guido Busca [b], Hassib Tounsi [a]

[a] Laboratoire des Matériaux Avancés, Ecole Nationale d'Ingénieurs de Sfax, Université de Sfax, Tunisia
[b] Dipartimento di Ingegneria Civile, Chimica e Ambientale (DICCA), Università degli Studi di Genova, Via Opera Pia 15, 16145, Genova, Italy
[c] ICGM, Univ Montpellier, ENSCM (MACS), CNRS, Montpellier, France

HIGHLIGHTS

- Valorizing waste glass and aluminum scraps at minimum energy consumption.
- Synthesis of zeolite using inexpensive materials.
- The conservation of raw materials is achieved by recycling wastes.
- The type of the obtained zeolite depends on the synthesis conditions.

GRAPHICAL ABSTRACT

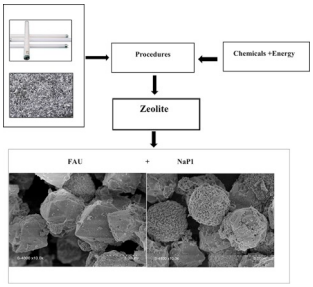

ARTICLE INFO

Keywords:
Valorization
Aluminum scraps
Fluorescent tube glass
Faujasite
NaP1 zeolite

ABSTRACT

The present work reports the feasibility of valorizing waste glass and aluminum scraps into zeotype materials. The raw materials were reacted hydrothermally at 60 °C using alkaline fusion prior to hydrothermal treatment. The obtained powders were characterized by X-ray diffraction (XRD), X-ray fluorescence (XRF), Fourier transform infrared spectroscopy (FTIR), electron microscopy (SEM) and magic angle spinning nuclear magnetic resonance (MAS NMR) of ^{27}Al and ^{29}Si nuclei. The influence of some parameters like alkalinity, reaction time and particle size on the nature of obtained zeolites has been also studied. The characterization methods demonstrated that the final products are aluminosilicate materials with a high cation exchange capacity containing Na-FAU and Na–P1 zeolites. The above results show that valorization of waste glass and aluminum scraps to obtain Na-FAU and NaP1 zeolites is possible and can be a sustainable alternative to the traditional synthesis methods.

1. Introduction

Recently, a growing attention has been paid to the development of eco-friendly procedure such as the reuse and the valorization of waste materials especially, those containing silicon- and aluminum to reduce the use of natural resources. Waste materials based silicon and aluminum can be transformed into porous materials like amorphous silicas, alumina, amorphous silica-alumina, and zeolites [1]. Several researches intended to use low-cost, raw materials to prepare zeolites [2]. Those zeotype materials are microporous solids, with 3-dimensional framework of $[SiO_4]^{4-}$ and $[AlO_4]^{5-}$ tetrahedra linked at their corners. This structure generated pores and channels with molecular dimensions

* Corresponding author.
E-mail address: sayahimouna@gmail.com (M. Sayehi).

https://doi.org/10.1016/j.matchemphys.2020.122903
Received 14 January 2020; Received in revised form 2 March 2020; Accepted 3 March 2020
Available online 7 March 2020

which confer to zeolites sieving molecular properties and high thermal, mechanical and chemical stability. Due to their interesting properties, zeolites can be useful in many industrial fields such as catalysis [3], water treatment [4], detergent builders adsorbents, agricultural application [5], biotechnology and medicine [6]. Inexpensive materials are mainly clays [7–10], volcanic glasses [11], Tunisian sand [12,13] or industrial waste products as coal fly, bagasse fly ash [9,14,15], waste sanitary porcelain [16], waste aluminum cans [17], aluminum scraps [12,18,19] and glass wastes [20–27]. The first study conducted to prepare porous materials (ANA and GIS zeolites) was completed using waste bottle glass [28]. Industrial raw powder glass was used in 2014 by Alves et al. [29] to prepare zeolite LTA, X and HS. Alves et al. [30] used the alkaline fusion followed by a hydrothermal treatment technique since the glass powder residue is difficult to zeolitize by hydrothermal treatment in basic media. Kim et al. [31] successfully synthesized uniform-sized LTA zeolite from windshield waste via high-energy ball milling and a low-temperature hydrothermal process. Terzano et al. [27] showed the facile zeolite synthesis from municipal glass and aluminum solid wastes. The e-wastes like LCD panel glass [23] and cathode-ray-tube funnel glass [22] were also used in the preparation of LTA, FAU and NaP1 zeolites. Zeolite HS and NaP1 were prepared using microwave radiation from residue called waste glass cullet [24–26]. On the other hand, Vinaches et al. [32,33] used fluoride media for the zeolitization of raw powder glass to ZSM-5 and MEL zeolites.

The rapid increase in production and usage of fluorescent tubes and aluminum led to the high volume of wastes discharged that presents risks on the environment and on humans' health. The average number of end-of-life fluorescent lamps generated each year, reached about 3.8 tubes per person in Taiwan [34] and the world production of aluminum was about 314,616 thousand metric tons for December 2014 to December 2019 [35]. In order to minimize their discharge as well as their negative impacts on the environment, developing more sustainable alternatives is essential. To the best of our knowledge, there are no previous studies related to the co-valorization of glass waste from fluorescent tube and aluminum scraps into zeolite materials. In this manner, our work aimed to develop a simple low-cost process for the synthesis of high added-value zeotype materials and to understand the influence of some parameters like alkalinity, reaction time and particle size on the nature of obtained zeolites.

2. Experimental procedure

2.1. Zeolite preparation

The aluminum source is scraps collected from aluminum workshop and the silica source was obtained by crushing the glass of the end-of-life fluorescent tubes collected from the special containers established by the administration of the National Engineering School of Sfax-Tunisia for the collection of hazardous waste. Various particle sizes of glass powder (63 μm, 125 μm and 315 μm) as average particle diameter were used in this procedure. The chemical composition of the WG was as follows: SiO_2-64.6%, Na_2O-21.5%, CaO-6.9%, MgO-3.0%, Al_2O_3-2.5%, K_2O-0.83%, Fe_2O_3-0.2%, SO_3-0.12% and TiO_2-0.06%. The chemical composition of aluminum scraps (AS) is Al-99,77% with very small quantities of iron Fe-0.207% and copper Cu-0.08%. Analytical grade NaOH pellets was purchased from Sigma Aldrich and 98%.

The alkaline fusion technique followed by the treatment has been chosen for the zeolitization of the WG. This technique consists of heating various NaOH/WG mixtures with different mass ratios ($R_1 = 0.8$; $R_2 = 1.0$ and $R_3 = 1.2$) at 550 °C for 1h in a nickel crucible. The fused products are named FP-R-y with ***R*** referred to the NaOH/WG mass ratio and ***y*** the particle size of the WG (63 μm; 125 μm; 315 μm). After fusion, the obtained product was cooled, ground again and mixed with 80 mL of sodium aluminate solution (SAS); L/S = 10. It is mentioned that the SAS was obtained by dissolving 0.5 g of aluminum scraps (AS) into 80 mL of 2.5 mol/L aqueous solution of NaOH. The mixture was vigorously stirred at room temperature (RT) for 2h and then let reacting in an oven for 6 days at 60 °C. At the end of the process, the solid was separated by filtration and washed thoroughly several times with deionized water until pH 9. The precipitated solid was dried at 80 °C for one night. The synthesized products are named ZFP-R-y with ***R*** referred to the NaOH/WG mass ratio (0.8; 1.0; 1.2) and ***y*** the particle size of the WG (63 μm; 125 μm; 315 μm) (Fig. 1).

2.2. Characterization

The wastes, the fused products and the prepared zeolites were characterized by different techniques. X-ray fluorescence (XRF) was used to assess chemical composition of the WG using Philips X'UNIQUE II apparatus. The chemical composition of the aluminum scraps was analyzed by NITON XL3t GOLDD de THERMO. Structural phase analysis by X-ray diffraction (XRD) was performed on a D8 AXS (DRX-Bruker D8) diffractometer, using Cukaα radiation (λ = 1.540598) in which the Bragg angle (2θ) was scanned from 5° to 50°. FTIR spectra of the samples were recorded in air at RT using attenuated total reflectance Fourier transform infrared spectroscopy (ATR-FTIR). The spectra were recorded using a PerkinElmer Fourier transform infrared spectrometer in the wave-number range 4000–400 cm^{-1}. The examination of the morphology of both raw materials and solid products was investigated by scanning electron microscopy (SEM) with a JEOL JSM-5400 instrument. Samples were mounted on suitable substrates using a conductive glue, then coated with a thin layer of gold to make them conductive.

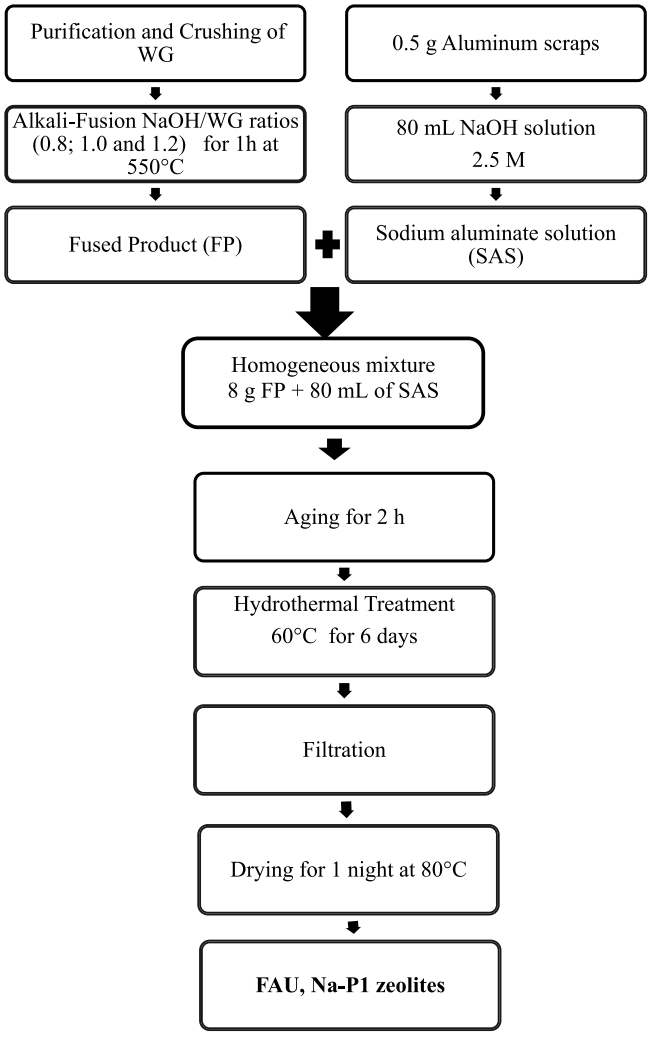

Fig. 1. Schematic diagram of Zeolite synthesis.

Physisorption isotherms were measured at −196 °C on a Micromeritics ASAP 2020 instrument with nitrogen as probe molecule. Prior to measurement the samples were degassed for 12 h at 200 °C before adsorption. ^{27}Al and ^{29}Si MAS-NMR spectra were recorded on a Brucker 300 MHz (AMX 300) at 78.20 and 58.48 MHz, respectively. The chemical shift in ppm was obtained with respect to $AlCl_3{\cdot}6H_2O$ and TMS as external references for Al and Si, respectively. Particle size distribution (PSD) of the samples was determined by laser diffraction particle size analyzer type Malvern Instruments Ltd 3000. The powders were dispersed in distilled water. The solution was ultrasonicated for few minutes on auto basis to disaggregate the agglomerate before the start of test run. The instrument computed average of three runs to ensure precision. The standard volume percentiles at 10, 50, and 90, denoted as D10, D50 and D90, respectively, were recorded from the analysis and used to calculate the width of the distribution span [36].

$$span = \frac{D_{90} - D_{10}}{D_{50}}$$

where D_{10}, D_{50} and D_{90}: the 10th, 50th and 90th percentiles of the Average grain diameters.

3. Results and discussion

3.1. Characterization of the fused waste

The X-ray diffraction patterns of the fused products using different NaOH/WG ratios are reported in Fig. 2. The fusion step at 550 °C for 1h facilitates the formation of soluble silicate and aluminate salts which are crystallized afterward into zeolites by the hydrothermal treatment. Indeed, the XRD profiles show the decrease of the amorphous content of the WG and the appearance of new peaks related to crystalline phases. The phase identification was carried out using X'Pert High Score Plus software. Table 1 summarized the different solids found in the fused products after the fusion step. The mainly compounds detected are the sodium silicates **$Na_3HSiO_4(H_2O)_2$** and **Na_4SiO_4** regardless the NaOH quantity. This result is expected since the SiO_2/Al_2O_3 molar ratio of the WG is about 43. Accordingly, the peaks detected at 2θ 16.89°, 17.52°, 18.96°, 29.34°, 32.22°, 34.91° and 37.54°are related to trisodium hydrogen silicate dihydrate **$Na_3HSiO_4(H_2O)_2$** and the peaks of sodium orthosilicate **Na_4SiO_4** appeared at 18.96°, 34.91°, 37.35° and 42.73°. Besides, slight amount of **$NaAlSi_2O_6$** (JCPDS No.01-071-1507) is also detected for **FP-0.8–125** and **FP-1.0–125** samples (30.28°, 31.03°, 35.98°and 36.73°). When the NaOH quantity is increased for samples

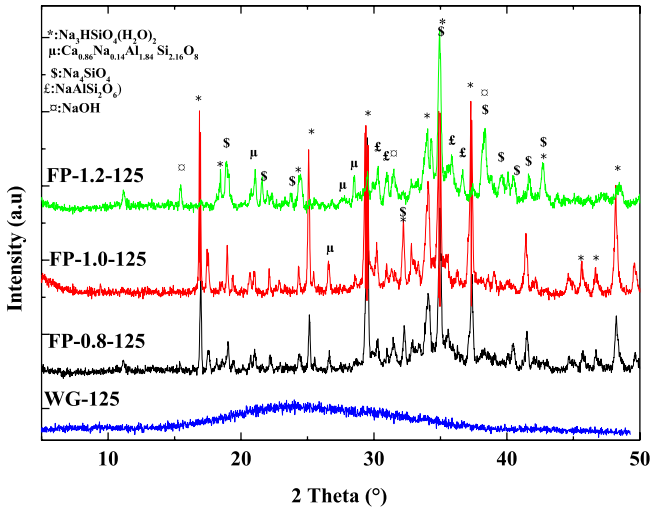

Fig. 2. XRD patterns of the WG and the three fused products after the fusion step at 550 °C for 1h.

FP1.0–125 and **FP-1.2–125**, there is appearance of sodium calcium silicoaluminate **$Ca_{0.86}Na_{0.14}Al_{1.84}Si_{2.16}O_8$** (21.08°, 26.59°, 27.72° and 28.72°). The residual NaOH with peaks at 15.51°, 31.47° and 38.36° can be related to the excess of NaOH used for the alkaline fusion [16,37,38].

The FTIR spectra of the fused products displayed significant changes in relative intensities and width of vibration bands compared to WG spectrum (Fig. 3). There is a shift of the large band at 1050 cm^{-1} attributed to asymmetric stretching vibration of the Si–O groups in the WG to lower wavenumber at 925–1200 cm^{-1} [16,39]. This result confirms the formation of silicate and aluminosilicate salts as showed by XRD technique. It should be mentioned that the fused products contain carbonate species confirmed by the presence of the peaks at 1450 cm^{-1} and 880 cm^{-1}.

3.2. Influence of NaOH/WG ratio on the nature of the obtained zeolites

To investigate the effect of NaOH/WG mass ratio on the resulting zeolite products, three mixtures (**$R_1 = 0.8$, $R_2 = 1.0$ and $R_3 = 1.2$**) were tested using WG powder with a particle size Ø < 125 μm (WG-125). The XRD patterns of the recovered solids after hydrothermal treatment at 60 °C for 6 days were illustrated in Fig. 4. The phase identification was carried out using X'Pert High Score Plus software. The analysis of the diffraction patterns shows that **ZFP-0.8–125 and ZFP-1.0–125** samples, contain a mixture of zeolite faujasite at 6.16°, 10.02°, 11.80°, 15.51°, 20.02° and 23.39° ($|Na_{4.43}(H_2O)_{8.882}|[Al_6Si_6O_{24}]$; JCPDS N°01-072-2421) and the so-called zeolite Na–P1 ($|Na_6(H_2O)_{12}|$ $[Al_6Si_{10}O_{32}]$; JCPDS N°01-071-096). The sample **ZFP-1.2–125** contains mainly the zeolite Na–P1 (2θ 12.53°; 21.76°; 28.12° and 33.48°). The analysis of the diffraction patterns showed that the nature of the prepared zeolite depends on the NaOH/WG ratio. The increase of the NaOH amount from $R_1 = 0.8$ to $R_2 = 1.0$ had no important effect on zeolite crystallization [40]. For ZFP-1.2-125 sample, the increase of the mass ratio favors the formation of Na–P1 zeolite at the expense of FAU zeolite. This result can be explained by the influence of the residual amount of NaOH on the alkalinity of the solution. Volli et al. [41] showed that with the increase in NaOH concentration; in the case of the zeolitization of fly ash; there is an increase in supersaturation which could change the type of zeolite. According to Ostwald's rule of successive transformation, the higher the supersaturation, better the condition to nucleate metastable phases, such as zeolite FAU, which later recrystallizes and is replaced by highly stable zeolite Na–P1.

The SEM micrographs with different magnifications of the synthesized samples are reported in Fig. 5. The micrographs of **ZFP-0.8–125** and **ZFP-1.0–125** display the presence of co-phase. The octahedral particles characterize the morphology of zeolite FAU [42,43] and the spherical ones the zeolite Na–P1 [44]. The magnified micrographs indicate that NaP1 zeolite exhibits knobbed surface microspheres composed of crystalline nanoparticles. For the solid **ZFP-1.2–125**, the influence of residual alkalinity is clear; the formed zeolite FAU tends to dissolve and re-crystallize during the experiment to zeolite Na–P1.

PSD of the samples **ZFP-0.8–125**, **ZFP-1.0–125** and **ZFP-1.2–125** are illustrated in Fig. 6. All samples present multimodal distribution in which the particle size varies in the range of 0.3–200 mm. Table 2 reports the granulometric parameters of the samples. For **ZFP-0.8–125** sample, one can distinguish three distinct populations. The first one is situated in the range of 0.2–1.0 μm with mode M1 = 0.46 μm and represents 11%. The second population which represents 24% had particle size in the range of 1.0–5 μm with mode M2 = 2.13 μm. The last population with mode M3 = 34.53 μm lies from 5 to 170 μm and represents 65%. The influence of the alkalinity is clearly visible; the increase in the NaOH/WG ratio shifted the particle size distribution curves to bigger particle sizes. It seems that the residual alkalinity leads to the agglomeration of the zeolite particles.

The ^{27}Al MAS-NMR spectra of the WG and of the zeotype materials are reported in Fig. 7 a. ^{27}Al MAS-NMR spectrum of WG displays a broad peak at 55.2 ppm with full-width-at-half-maximum (FWHM) of about

Table 1
Quantitative analysis of the fused products.

Compound	$NaAlSi_2O_6$ (%)	$Na_3HSiO_4(H_2O)_2$ (%)	Na_4SiO_4 (%)	$Ca_{0.86}Na_{0.14}Al_{1.84}Si_{2.16}O_8$ (%)	NaOH (%)
JCPDS N°	01-071-1507	01-074-0667	01-078-1432	01-076-0832	01-078-0189
FP-0.8-125	7	71	18	–	–
FP-1.0-125	5	42	26	25	2
FP-1.2-125	–	35	38	18	9

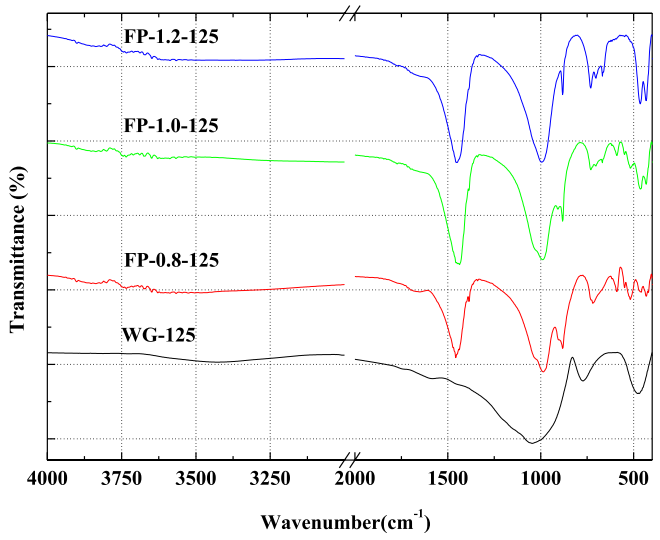

Fig. 3. Infrared spectra of the fused products.

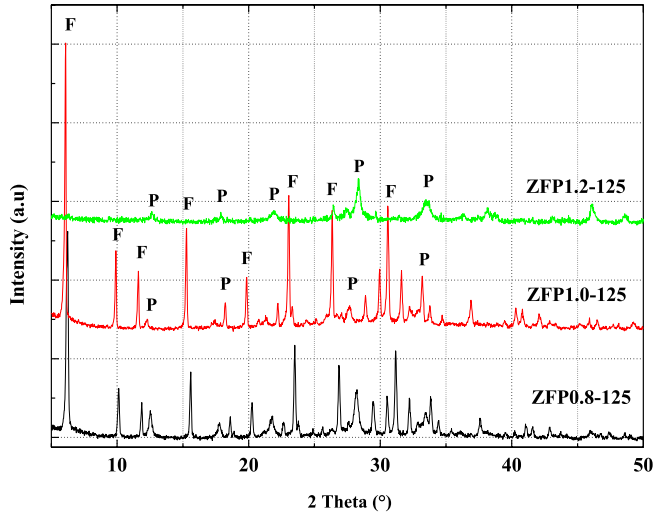

Fig. 4. Zeolites obtained by alkaline fusion followed by hydrothermal treatment.

25 ppm. This peak is typical of aluminum atoms in a tetrahedral coordination, which is broadened to the more shielded side of the peak. After the zeolitization of the fused product, the samples **ZFP-0.8–125**, **ZFP-1.0–125** and **ZFP-1.2–125** exhibit strong peaks centered at 57–58 ppm ascribed to the aluminum atoms in a tetrahedral coordination [45]. For **ZFP-1.2–125**, an additional peak was observed at 10 ppm which may indicate the presence of another phase beside zeolite having the aluminum in octahedral environment. ^{27}Al MAS-NMR technique confirms the results of XRD and SEM in which the formed zeolite FAU tends to dissolve and re-crystallize during the experiment to zeolite Na–P1 [46]. The ^{29}Si MAS-NMR spectra of the WG and samples **ZFP-0.8–125**, **ZFP-1.0–125** and **ZFP-1.2–125** are reported in Fig. 7 b the spectrum of the WG shows a broad peak (FWHM = 21 ppm) centered about −92 ppm with shoulder at about −103 ppm. According to the chemical shift ranges and the large amount of alkalis ($Na_2O + K_2O$ = 22.33%) in the WG, one can assume that the majority of silicon species are of type Q^2 and Q^3. After the zeolitization of the WG, one can see clear changes in the ^{29}Si MAS-NMR spectra of **ZFP-0.8–125**, **ZFP-1.0–125** and **ZFP-1.2–125** samples. **ZFP-0.8–125** and **ZFP-1.0–125** show five peaks centered at ca. −87, −91, −97, −102 and −107 related to the respective Q^4 Si coordination environments Si(4Al), Si(3Al), Si(2Al), Si(1Al) and Si (0Al) [47]. For the sample ZFP-1.2-125, despite the bad resolution one can distinguish three peaks at about ca. −85, −89, −92 ppm. On the other hand, it is possible to calculate the framework Si/A1 ratio according to the equation [48]:

$$\frac{Si}{Al} = \frac{\sum_{n=0}^{4} I_{Si(nAl)}}{\sum_{n=0}^{4} 0.25 \times n \times I_{Si(nAl)}}$$

where $I_{Si(nAl)}$ is the intensity of a ^{29}Si MAS NMR peak. The corresponding to the Si(*n*Al) unit.

The Si/Al molar ratio determined by ^{29}Si-NMR of ZFP-0.8-125 is about 1.44, which is in good agreement with the Si/Al ratios of the FAU zeolites. Increasing the amount of sodium hydroxide (ZFP-1.0-125) increases the Si/Al ratio from 1.44 to 1.67.

The FTIR spectra of the WG and prepared zeolites **ZFP-0.8–125**, **ZFP-1.0–125** and **ZFP-1.2–125** are summarized in Fig. 8. The large band centered at 1050 cm^{-1} attributed to asymmetric stretching vibration of the Si–O groups in the WG was shifted to lower wavenumber at 925–1200 cm^{-1} and became sharper [39]. The band at around 1005 cm^{-1} could be assigned to asymmetric stretching of T–O bonds (T = Si or Al) in zeolites, whereas the symmetrical stretching of T–O bonds is situated at 750 cm^{-1}. The bands near 668 cm^{-1} and 740 cm^{-1} are ascribed to a symmetric stretch of internal tetrahedra as well as of external linkages. The band related to T-O bending mode in aluminosilicate zeolites is present near 445 cm^{-1}. The bands at higher wavenumbers 3450 cm^{-1} can be assigned to stretching vibrations of *O*–H bonds whereas the bands at around 1652 cm^{-1} to bending vibrations of water molecules. In zeolite materials, the 800-500 cm^{-1} region is related to the bands originating from structural units, like S4R, S6R, D4R and D6R rings [49]. Thus, the bands at 600 cm^{-1} and 610 cm^{-1} for **ZFP-0.8–125** and **ZFP-1.0–125**, respectively were assigned to the vibrations of tetrahedra from external linkages of the double six rings (D6R) in the framework of zeolite Na-FAU. The presence of two bands at about 740 cm^{-1} and 668 cm^{-1} associated with four-membered ring vibrations occurring both in the structure of Na-FAU and Na–P1 zeolites. The absorption band at 569 cm^{-1} of ZFP-1.2-125 is due to the S4R T–O–T symmetric stretching of Na–P1 zeolite [50]. The band centered at about 1450 cm^{-1} may represent the vibration of carbonate species.

The N_2 adsorption-desorption isotherms of ZFP-0.8-125, ZFP-0.1-125 and ZFP1.2-125 samples are reported in Fig. 9. Table 3 summarizes the results of BET specific surface areas (S_{BET}), microporous surface (S_{mic}), external surface (S_{ext}), microporous volume (V_{mic}), total volume (V_{tot}) and BJH pore diameter ($Ø_{pore}$) of the prepared samples. The adsorption-desorption isotherms can be classified roughly as IV type with hysteresis loop. The presence of micropores cannot be excluded

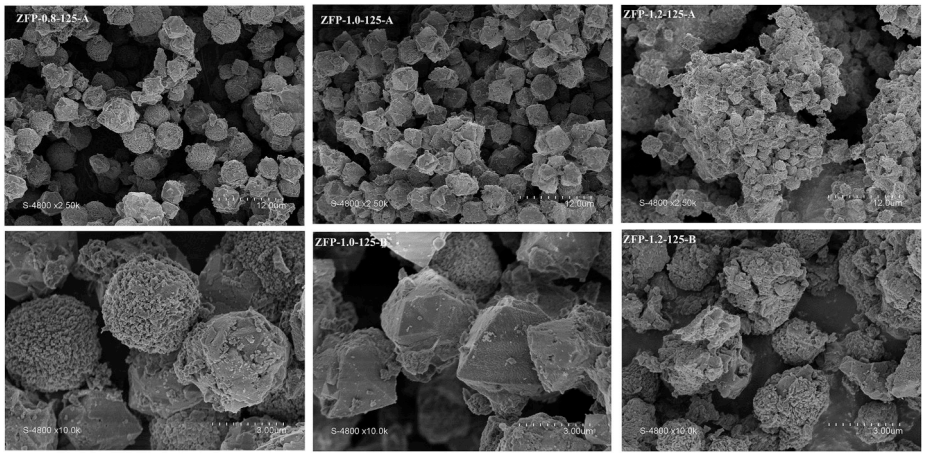

Fig. 5. SEM photomicrographs of **ZFP-0.8-125**, **ZFP-1.0-125** and **ZFP-1.2-125** samples at different magnifications.

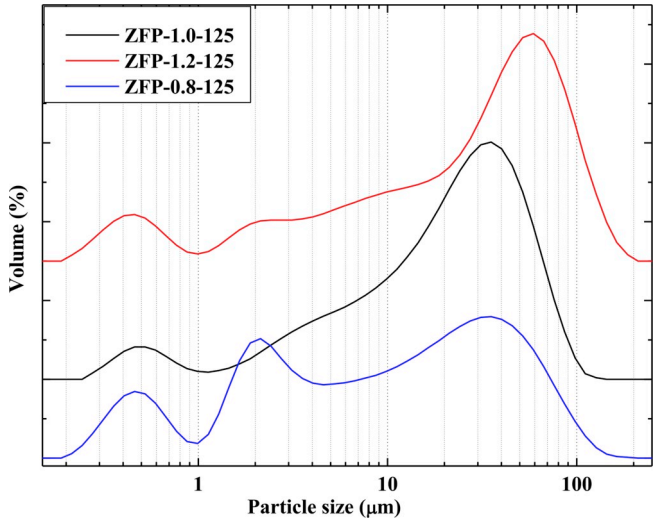

Fig. 6. PSD of the samples **ZFP-0.8-125**, **ZFP-1.0-125** and **ZFP-1.2-125**.

Table 2
Granulometric parameters of the obtained zeolites **ZFP-0.8-125**, **ZFP-1.0-125** and **ZFP-1.2-125**.

Samples	ZFP-0.8-125	ZFP-1.0-125	ZFP-1.2-125
D10 (μm)	0.71	3.21	1.70
D50 (μm)	11.5	23.9	35.5
D90 (μm)	59.4	60.4	96.2
Span	5.1	2.4	2.7
M1 (μm)	0.46	0.50	0.45
M2 (μm)	2.13	3.61	2.00
M3 (μm)	34.53	35.09	59.50

since at very low relative pressures ($P/P_0 = 0.02$), there is a steep in the nitrogen uptake attributed to the filling of micropores. But the presence of hysteresis loop observed at high relative pressures indicates that the samples contain mesopores. The mesoporous character may arise from the assembling of the nano-size crystallites that composed the zeolite Na–P1 microspheres. The hysteresis loop is type H4 for ZFP-1.2-125 and type H3 for ZFP-1.0-125, ZFP-0.8-125. These loops correspond to the filling of uniform slit-shaped inter-crystal mesopores or of non-rigid aggregates of plate-like particles. On the other hand, the measured S_{BET} of the zeolites ZFP-1.0-125, ZFP-0.8-125 and ZFP-1.2-125 are 392 $m^2\ g^{-1}$, 329 $m^2.g^{-1}$and 24 $m^2\ g^{-1}$, respectively. The low S_{BET} value for ZFP-1.2-125 is due to the inappropriate use of nitrogen as adsorbent to

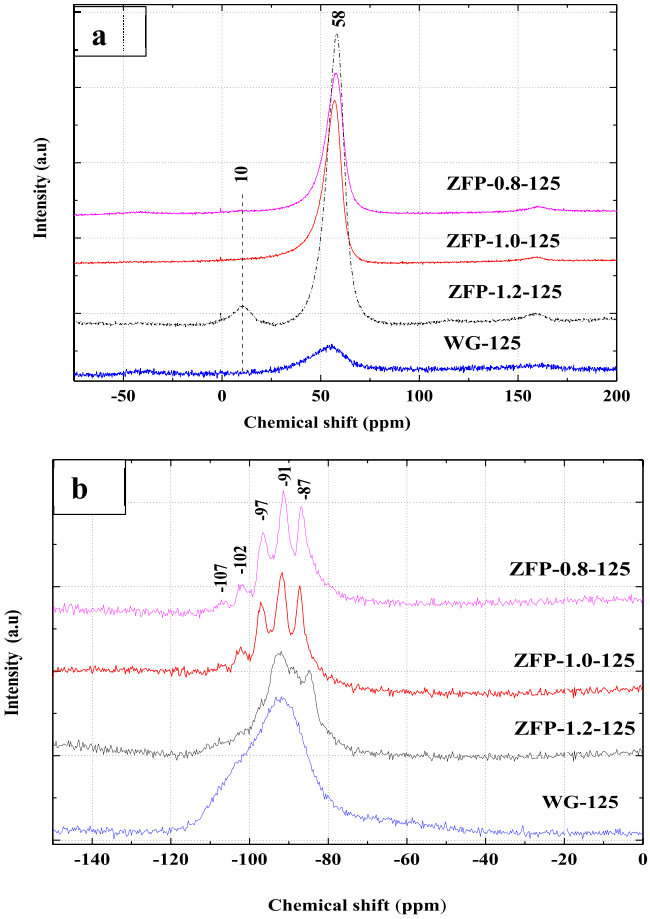

Fig. 7. ^{27}Al MAS NMR(a) and ^{29}Si MAS NMR (b)spectra of the WG-125 and the recovered solids after hydrothermal treatment **ZFP-0.8-125**, **ZFP-1.0-125** and **ZFP-1.2-125**.

assess the textural properties of zeolite Na–P1 (ZFP-1.2-125). The framework of Na–P1 zeolite contains small micropores (ultra-micropores < 0.7 nm) which are not accessible for nitrogen [45]. For the samples ZFP-1.0-125, **ZFP-0.8–125**, the measured S_{BET} are consistent for FAU zeolites. Zeolite **ZFP-1.0–125** has the highest S_{BET} compared to **ZFP-0.8–125** because it has the lowest amount of Na–P1 zeolite.

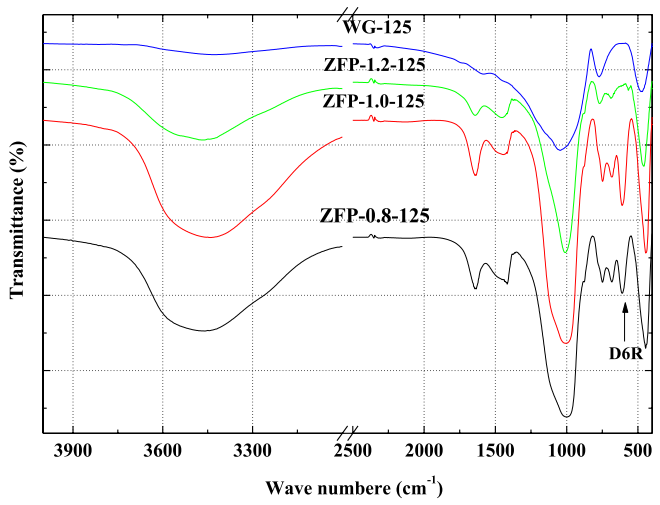

Fig. 8. Infrared spectra of WG-125 and the recovered solids products **ZFP-0.8-125**, **ZFP-1.0-125** and **ZFP-1.2-125**.

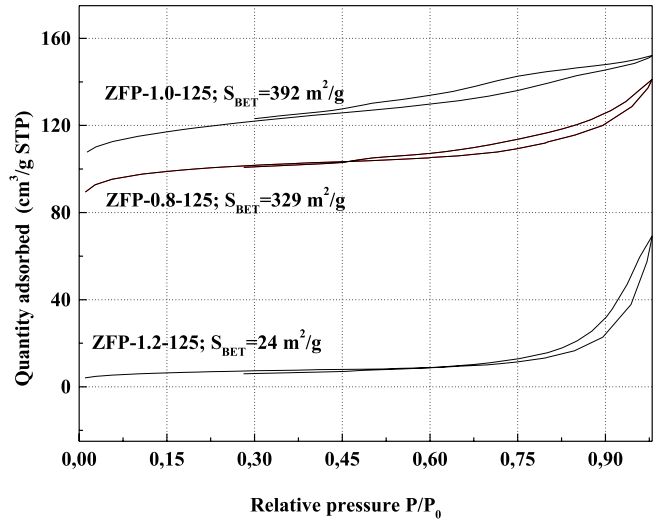

Fig. 9. Nitrogen adsorption–desorption isotherms of **ZFP-0.8-125**, **ZFP-1.0-125** and **ZFP-1.2-125** samples.

3.3. Influence of the reaction time

Fig. 10 shows the XRD patterns of the synthesized samples obtained at different crystallization periods at 60 °C obtained from NaOH/WG ratio $R_1 = 0.8$ using WG-125. The X-ray profile of the solid obtained after 2 days of hydrothermal treatment (ZPF-0.8-2d) shows a broad hump in the baseline between about 15 and 35° 2θ, which is related to the presence of amorphous aluminosilicate gel. After 4 days, one can see the development of the new peaks relative to crystalline phases and the decrease of the quantity of amorphous phase. Indeed, the peaks can be associated to zeolite Na-FAU (6.16°, 10.02°, 11.80°, 15.51°, 20.02° and 23.39°) and Na–P1 (12.53°; 21.76°; 28.12° and 33.48°). After 6 days of crystallization, the amorphous phase totally disappears in favor of the crystalline phases. The peak intensities of zeolite Na–P1 increase after the prolonged crystallization period up to 6 days [42]. In Table 4, is reported the zeolite quantification as function of time from 6 to 10 days. The relative quantity of NaP1 phase increased from 42% for ZPF-0.8-6d to 80% for ZPF-0.8-10d. The transformation of the metastable phase; zeolite Na-FAU to more thermodynamically stable phase zeolite Na–P1 at longer reaction time can be explained by Ostwald's rule of successive transformations. It is well known that zeolite formation is a kinetically

Table 3
BET specific surface areas (S_{BET}), microporous surface (S_{mic}), external surface (S_{ext}), microporous volume (V_{mic}), total volume (V_{tot}) and BJH pore diameter ($Ø_{pore}$) of the prepared samples.

Samples	S_{BET} (m^2/g)	S_{mic} (m^2/g)	S_{ext} (m^2/g)	V_{mic} (cm^3/g)	V_{tot} (cm^3/g)	$Ø_{pore}$ (nm)
ZFP-0.8-63	40	12	29	0.005	0.115	12.7
ZFP-0.8-125	**329**	**276**	**53**	**0.131**	**0.200**	**8.7**
ZFP-0.8-315	12	9	3	0.004	0.039	9.2
ZFP-1.0-63	489	381	108	0.169	0.311	6.1
ZFP-1.0-125	**392**	**309**	**83**	**0.148**	**0.230**	**5.5**
ZFP-1.0-315	85	42	43	0.020	0.077	6.3
ZFP-1.2-63	51	21	30	0.010	0.067	9.2
ZFP-1.2-125	**24**	**7**	**17**	**0.003**	**0.062**	**16.7**
ZFP-1.2-315	62	36	26	0.017	0.079	6.7

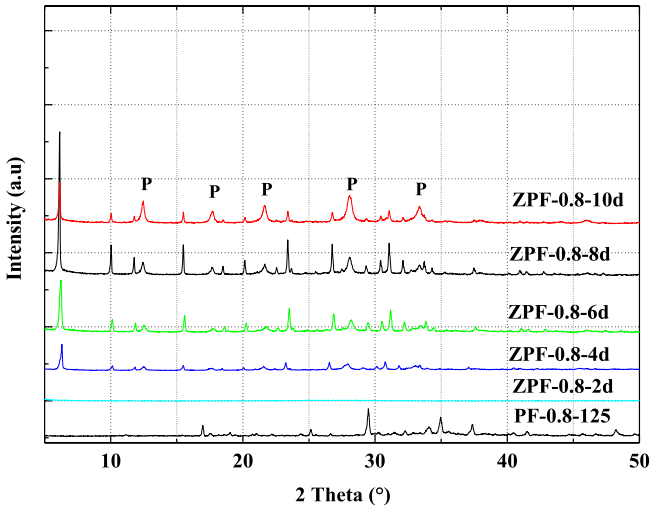

Fig. 10. XRD patterns of ZFP0.8 as function of time (2, 4, 6, 8 and 10 days).

Table 4
Quantification of **ZFP0.8-6d**, **ZFP0.8-8d** and **ZFP0.8-10d** samples.

Compound	JCPDS N°	ZFP-0.8-6d	ZFP-0.8-8d	ZFP-0.8-10d
Na-FAU (%)	01-076-0843	58	24	20
Na–P1 (%)	01-071-0962	42	76	80

controlled process and the reaction is generally stopped when the desired zeolite has formed. Extended reaction time at high temperature and/or high pressure usually results in dense phases. The new phase occurs in the supersaturated solution throughout the dissolution of the former phase [42].

3.4. Influence of the WG particle size

Fig. 11 illustrated the XRD patterns of the obtained zeolites when the particle sizes of the WG were varied from 63 μm to 315 μm for a constant NaOH/WG ratio; $R_2 = 0.8$. One can conclude that particle size of the WG controls the nature of the prepared zeolites. It seems that the increase of the WG particle size favors the formation of the zeolite Na–P1 whatever the NaOH/WG ratios (Figs. 12 and 13). On the other hand, Fig. 13

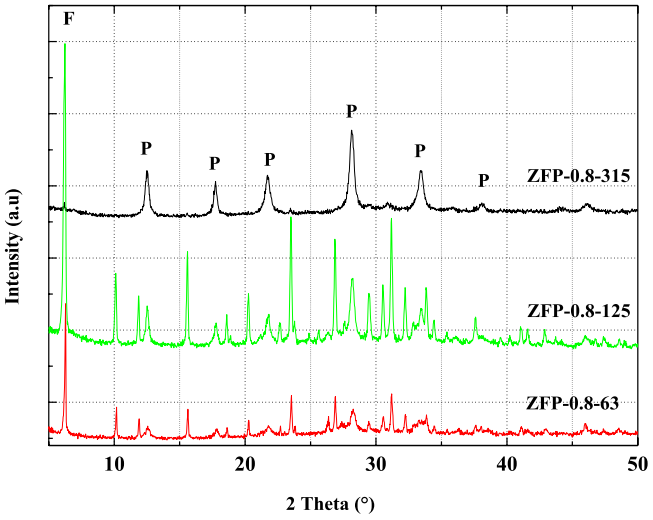

Fig. 11. XRD patterns of **ZFP-0.8-63**, **ZFP-0.8-125** and **ZFP-0.8-315**.

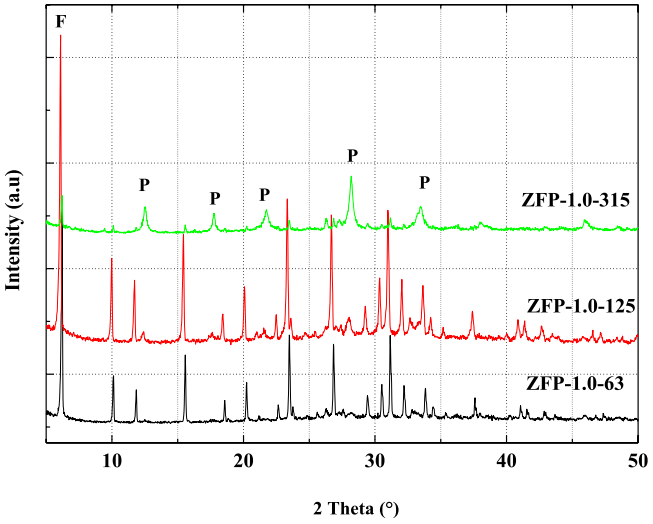

Fig. 12. XRD patterns of **ZFP-1.0-63**, **ZFP-1.0-125** and **ZFP-1.0-315**.

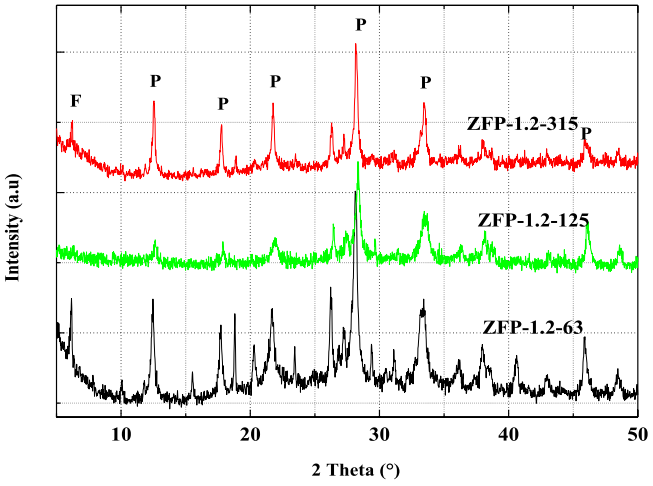

Fig. 13. XRD patterns of **ZFP-1.2-63**, **ZFP-1.2-125** and **ZFP-1.2-315**.

reveals that the increase of the NaOH quantity favors also the formation of the zeolite Na–P1 whatever the particle size.

SEM micrographs of the samples **ZFP-1.0-63**, **ZFP-1.0-125** and **ZFP-1.0-315** are reported in Fig. 14. It was shown that the product materials are zeolite type NaP1, contaminated with small amount of FAU zeolite with spherical shape [51]. The morphology contained wool ball-like ones expected for NaP1 zeolites with uniform size distribution 3 μm.

4. Conclusions

In this study, it was shown that valorizing WG and AS into high added value zeolites at minimum energy consumption is possible. Alkaline fusion prior to hydrothermal treatment was employed as recycling process. The results indicated that alkalinity, reaction time and particle size of the powder of WG have a significant role in zeolite synthesis. Increasing the NaOH/WG ratio from 0.8 to 1.0 and 1.2, favors the transformation of zeolite Na-FAU to Na–P1. The same transformation was showed by prolonging crystallization time from 2 to 10

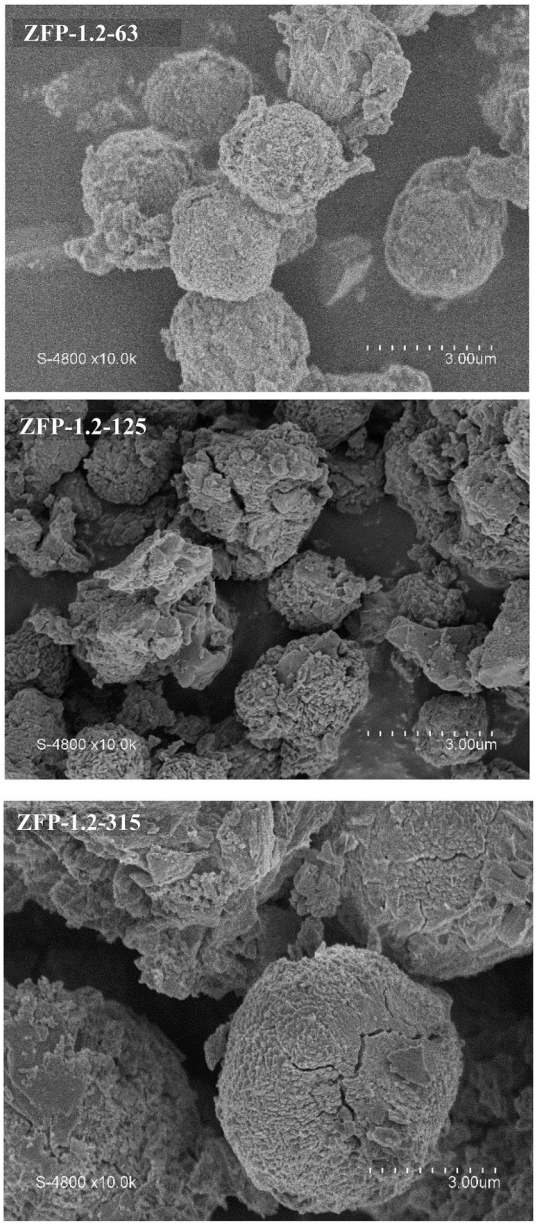

Fig. 14. SEM micrographs of zeolite obtained at NaOH/WG = 1.2 from various particle size.

days and increasing particle size form 63 μm–315 μm.

Declaration of competing interest

The authors declare that they have no known competing financial interests or personal relationships that could have appeared to influence the work reported in this paper.

CRediT authorship contribution statement

Mouna Sayehi: Investigation, Writing - original draft. **Gabriella Garbarino:** Methodology, Validation. **Gérard Delahay:** Formal analysis. **Guido Busca:** Validation, Conceptualization. **Hassib Tounsi:** Supervision.

References

[1] M. Sayehi, H. Tounsi, G. Garbarino, P. Riani, G. Busca, Reutilization of silicon- and aluminum- containing wastes in the perspective of the preparation of SiO 2 -Al 2 O 3 based porous materials for adsorbents and catalysts, Waste Manag. 103 (2020) 146–158, https://doi.org/10.1016/j.wasman.2019.12.013.

[2] R.C. Lima, L. Bieseki, P.V. Melguizo, S. Materials, Environmentally Friendly Zeolites, (n.d).

[3] R. Kumar, V. Strezov, E. Lovell, T. Kan, J. He, B. Dastjerdi, J. Scott, Nickel/zeolite and Copper-Nickel/zeolite catalysts, Bioresour. Technol. (2019), https://doi.org/10.1016/j.biortech.2019.01.067.

[4] M. Visa, PT, Elsevier B.V., 2016, https://doi.org/10.1016/j.powtec.2016.02.019.

[5] C. Gomes, H. Schneider, N. Romeu, L. Ferret, J. Carlos, P. Oliveira, Potassic Zeolites from Brazilian Coal Ash for Use as a Fertilizer in Agriculture, Waste Manag. (2017), https://doi.org/10.1016/j.wasman.2017.08.039.

[6] L. Bacakova, M. Vandrovcova, Biomaterials Science medicine – a review, Biomater. Sci. 6 (2018) 974–989, https://doi.org/10.1039/c8bm00028j.

[7] L. Yang, X. Qian, P. Yuan, H. Bai, T. Miki, F. Men, H. Li, T. Nagasaka, SC, J. Clean. Prod. (2019), https://doi.org/10.1016/j.jclepro.2018.11.259.

[8] T. Abdullahi, Z. Harun, M. Hafiz, D. Othman, A review on sustainable synthesis of zeolite from kaolinite resources via hydrothermal process A review on sustainable synthesis of zeolite from kaolinite resources via hydrothermal process, Adv. Powder Technol. 28 (2017) 1827–1840, https://doi.org/10.1016/j.apt.2017.04.028.

[9] T. Abdullahi, Z. Harun, M. Hafiz, D. Othman, A review on sustainable synthesis of zeolite from kaolinite resources via hydrothermal process, Adv. Powder Technol. (2017), https://doi.org/10.1016/j.apt.2017.04.028.

[10] M. Yoldi, S.A. Korili, A. Gil, Microporous and mesoporous materials zeolite synthesis from industrial wastes, Microporous Mesoporous Mater. 287 (2019) 183–191, https://doi.org/10.1016/j.micromeso.2019.06.009.

[11] C. Belviso, AC SC, Microporous Mesoporous Mater. (2016), https://doi.org/10.1016/j.micromeso.2016.01.048.

[12] H. Tounsi, S. Mseddi, S. Djemal, Hydrothermal synthesis of Na-LTA , Na-X and HS zeolites from, Tunisian Sand Alum. Scraps 637 (2010) 1389–1396. http://doi.org/10.4028/www.scientific.net/MSF.636-637.1389.

[13] H. Tounsi, S. Mseddi, S. Djemel, Preparation and characterization of Na-LTA zeolite from Tunisian sand and aluminum scrap, Phys. Procedia. 2 (2009) 1065–1074.

[14] O. Dere, O. Sabriye, A novel synthesis method of zeolite X from coal fly Ash : alkaline fusion followed by Ultrasonic-assisted synthesis method, Waste and Biomass Valorization 10 (2019) 143–154, https://doi.org/10.1007/s12649-017-0050-7.

[15] C. Wahyu, C. Salim, H. Hinode, Microporous and Mesoporous Materials Synthesis of pure Na – X and Na – a zeolite from bagasse fly ash, Microporous Mesoporous Mater. 162 (2012) 6–13, https://doi.org/10.1016/j.micromeso.2012.06.007.

[16] N. Maatoug, G. Delahay, H. Tounsi, Valorization of vitreous China waste to EMT/FAU, FAU and Na-P zeotype materials, Waste Manag. 74 (2018) 267–278.

[17] E.A. Abdelrahman, Synthesis of zeolite nanostructures from waste aluminum cans for efficient removal of malachite green dye from aqueous media, J. Mol. Liq. 253 (2018) 72–82, https://doi.org/10.1016/j.molliq.2018.01.038.

[18] H. Tounsi, S. Mseddi, S. Djemel, Preparation and characterization of Na-LTA zeolite from Tunisian sand and aluminum scrap, Phys. Procedia. 2 (2009) 1065–1074, https://doi.org/10.1016/j.phpro.2009.11.064.

[19] R. Abid, G. Delahay, H. Tounsi, Preparation of LTA , HS and FAU/EMT intergrowth zeolites from aluminum scraps and industrial metasilicate, J. Mater. Cycles Waste Manag. (2019), https://doi.org/10.1007/s10163-019-00873-x.

[20] M. Attari, S.S. Bukhari, H. Kazemian, S. Rohani, A low-cost adsorbent from coal fly ash for mercury removal from industrial wastewater, J. Environ. Chem. Eng. 5 (2017) 391–399.

[21] J.C. Kim, M. Choi, H.J. Song, J.E. Park, J.H. Yoon, K.S. Park, C.G. Lee, D.W. Kim, Synthesis of uniform-sized zeolite from windshield waste, Mater. Chem. Phys. 166 (2015) 20–25, https://doi.org/10.1016/j.matchemphys.2015.09.028.

[22] Z. Yao, D. Wu, J. Liu, W. Wu, H. Zhao, J. Tang, Recycling of typical difficult-to-treat e-waste: synthesize zeolites from waste cathode-ray-tube funnel glass, J. Hazard Mater. 324 (2017) 673–680, https://doi.org/10.1016/j.jhazmat.2016.11.041.

[23] M. Tsujiguchi, T. Kobashi, M. Oki, Y. Utsumi, N. Kakimori, A. Nakahira, Synthesis and characterization of zeolite A from crushed particles of aluminoborosilicate glass used in LCD panels, J. Asian Ceram. Soc. 2 (2014) 27–32, https://doi.org/10.1016/j.jascer.2013.12.005.

[24] A. Majdinasab, Q. Yuan, Microwave synthesis of zeolites from waste glass cullet using Landfill Leachate as a novel alternative solvent, Mater. Chem. Phys. (2018), https://doi.org/10.1016/j.matchemphys.2018.11.049.

[25] A.R. Majdinasab, Q. Yuan, Microwave synthesis of zeolites from waste glass cullet using indirect fusion and direct hydrothermal methods: a comparative study, Ceram. Int. (2018) 1–11, https://doi.org/10.1016/j.ceramint.2018.10.159.

[26] A.R. MaMannajdinasab, P.K.Y. Wroczynskyj, J. Van Lierop, N. Cicek, G. K. Tranmer, Cost-e ff ective zeolite synthesis from waste glass cullet using energy e ffi cient microwave radiation, Mater. Chem. Phys. 221 (2019) 272–287, https://doi.org/10.1016/j.matchemphys.2018.09.057.

[27] R. Terzano, C. D'Alessandro, M. Spagnuolo, M. Romagnoli, L. Medici, Facile zeolite synthesis from municipal glass and aluminum solid wastes, Clean - Soil, Air, Water 43 (2015) 133–140, https://doi.org/10.1002/clen.201400091.

[28] T. Takei, H. Ota, Q. Dong, A. Miura, Y. Yonesaki, Preparation of porous material from waste bottle glass by hydrothermal treatment, Ceram. Int. 38 (2012) 2153–2157, https://doi.org/10.1016/j.ceramint.2011.10.057.

[29] J. Alves, E.R.S. Dantas, S.B.C. Pergher, D.M. de A. Melo, M.A.F. Melo, Synthesis of high value-added zeolitic materials using glass powder residue as a silica source, Mater. Res. 17 (2014) 213–218.

[30] J.A.B.L. R, E.R. S, S.B. C, D.M. A, M.A. F, Synthesis of high value-added zeolitic materials using glass powder residue as a silica source 2, Exp. Proced. 17 (2014) 213–218.

[31] J.-C. Kim, M. Choi, H.J. Song, J.E. Park, J.-H. Yoon, K.-S. Park, C.G. Lee, D.-W. Kim, Synthesis of uniform-sized zeolite from windshield waste, Mater. Chem. Phys. 166 (2015) 20–25.

[32] P. Vinaches, E.P. Rebitski, J. Antônio, B.L.R. Alves, D.M.A. Melo, B.C. Sibele, Author ' s accepted manuscript study, Mater. Lett. (2015), https://doi.org/10.1016/j.matlet.2015.06.120.

[33] P. Vinaches, J.A.B.L.R. Alves, D.M.A. Melo, S.B.C. Pergher, Author ' s accepted manuscript, Mater. Lett. (2016), https://doi.org/10.1016/j.matlet.2016.05.006.

[34] H. Peng, S. Fang, K. Fan, T. Chang, Other Developed Countries, 2014, https://doi.org/10.1007/s10163-014-0253-y.

[35] International Aluminium Institute, Statistics, Available, (n.d.), http://www.world-aluminium.org/statistics/primary-aluminium-production/#data.

[36] H. Moghadam, M. Zakeri, A. Samimi, J. Part. Sci. Technol. 5 (2019) 71–76, https://doi.org/10.22104/JPST.2019.3455.1144.

[37] D. Ma, Z. Wang, M. Guo, M. Zhang, J. Liu, Feasible conversion of solid waste bauxite tailings into highly crystalline 4A zeolite with valuable application, Waste Manag. 2 (2014) 4–11, https://doi.org/10.1016/j.wasman.2014.07.012.

[38] A.R. Majdinasab, P.K. Manna, Y. Wroczynskyj, J. van Lierop, N. Cicek, G. K. Tranmer, Q. Yuan, Cost-effective zeolite synthesis from waste glass cullet using energy efficient microwave radiation, Mater. Chem. Phys. 221 (2019) 272–287, https://doi.org/10.1016/j.matchemphys.2018.09.057.

[39] Z. Jiang, J. Yang, H. Ma, L. Wang, X. Ma, Reaction behaviour of Al 2 O 3 and SiO 2 in high alumina coal fly ash during alkali hydrothermal process, Trans. Nonferrous Metals Soc. China 25 (2015) 2065–2072, https://doi.org/10.1016/S1003-6326(15)63816-X.

[40] S. Rayalu, S.U. Meshram, M.Z. Hasan, Highly Crystalline Faujasitic Zeolites from Flyash, J. Hazard Mater. (2000) 123–131.

[41] V. Volli, M.K. Purkait, Selective preparation of zeolite X and A from flyash and its use as catalyst for biodiesel production selective preparation of zeolite X and A from flyash and its use as catalyst for biodiesel production, J. Hazard Mater. 297 (2015) 101–111, https://doi.org/10.1016/j.jhazmat.2015.04.066.

[42] H. Tounsi, S. Mseddi, S. Djemal, Hydrothermal Synthesis of Na-LTA , Na-X and HS Zeolites from Tunisian Sand Hydrothermal Synthesis of Na-LTA , Na-X and HS Zeolites from Tunisian Sand and Aluminum Scraps, 2015. http://doi.org/10.4028/www.scientific.net/MSF.636-637.1389.

[43] C. Science, Selective formation of Na-X zeolite from coal fly ash by fusion with sodium hydroxide prior to hydrothermal reaction, J. Mater. Sci. 28 (1993) 4781–4786.

[44] P. Sharma, J. Song, M.H. Han, C. Cho, GIS-NaP1 zeolite microspheres as potential water adsorption material : influence of initial silica concentration on adsorptive and physical/topological properties, Nat. Publ. Gr. (2016) 1–26, https://doi.org/10.1038/srep22734.

[45] Z. Huo, X. Xu, Z. Lü, J. Song, M. He, Z. Li, Q. Wang, L. Yan, Microporous and mesoporous materials synthesis of zeolite NaP with controllable morphologies, Microporous Mesoporous Mater. 158 (2012) 137–140, https://doi.org/10.1016/j.micromeso.2012.03.026.

[46] D. Ruen-ngam, D. Rungsuk, R. Apiratikul, D. Ruen-ngam, D. Rungsuk, Zeolite Formation from Coal Fly Ash and its Adsorption Potential Zeolite Formation from Coal Fly Ash and its Adsorption Potential, 2012, p. 2247, https://doi.org/10.3155/1047-3289.59.10.1140.

[47] A. Miku, M. Kr, Microporous Mesoporous Mater. Synth. Zeolite Granulate Potential Sorption Appl. 243 (2017) 201–205, https://doi.org/10.1016/j.micromeso.2017.02.028.

[48] Solid-State NMR Characterization of Framework Structure of Zeolites and Zeotype Materials, n.d, Lect. Notes Chem. (2019), https://doi.org/10.1007/978-981-13-6967-4.

[49] A. Nezamzadeh-ejhieh, E. Mirzaeyan, Hexadecylpyridinium surfactant modi fi ed zeolite A as an active component of a polymeric membrane sul fi te selective

electrode, Mater. Sci. Eng. C 33 (2013) 4751–4758, https://doi.org/10.1016/j.msec.2013.07.040.
[50] S.N. Azizi, A.A. Daghigh, M. Abrishamkar, Phase Transformation of Zeolite P to Y and Analcime Zeolites Due to Changing the Time and Temperature, 2013, p. 2013.
[51] I.O. Ali, S.M. El-Sheikh, T.M. Salama, M.F. Bakr, M.H. Fodial, Controllable synthesis of NaP zeolite and its application in calcium adsorption, Sci. China Mater. 58 (2015) 621–633, https://doi.org/10.1007/s40843-015-0075-9.